



HAL
open science

Nanoscale characterization of collagen structural responses to in situ loading in rat Achilles tendons

Isabella Silva Barreto, Maria Pierantoni, Malin Hammerman, Elin Törnquist, Sophie Le Cann, Ana Diaz, Jonas Engqvist, Marianne Liebi, Pernilla Eliasson, Hanna Isaksson

► **To cite this version:**

Isabella Silva Barreto, Maria Pierantoni, Malin Hammerman, Elin Törnquist, Sophie Le Cann, et al.. Nanoscale characterization of collagen structural responses to in situ loading in rat Achilles tendons. Matrix Biology, 2023, 115, pp.32 - 47. 10.1016/j.matbio.2022.11.006 . hal-03888281

HAL Id: hal-03888281

<https://hal.science/hal-03888281>

Submitted on 7 Dec 2022

HAL is a multi-disciplinary open access archive for the deposit and dissemination of scientific research documents, whether they are published or not. The documents may come from teaching and research institutions in France or abroad, or from public or private research centers.

L'archive ouverte pluridisciplinaire **HAL**, est destinée au dépôt et à la diffusion de documents scientifiques de niveau recherche, publiés ou non, émanant des établissements d'enseignement et de recherche français ou étrangers, des laboratoires publics ou privés.



Nanoscale characterization of collagen structural responses to *in situ* loading in rat Achilles tendons



Isabella Silva Barreto^a, Maria Pierantoni^a, Malin Hammerman^{a,b}, Elin Törnquist^a, Sophie Le Cann^c, Ana Diaz^d, Jonas Engqvist^e, Marianne Liebi^{d,f,g}, Pernilla Eliasson^{b,h} and Hanna Isaksson^a

a - Department of Biomedical Engineering, Lund University, Lund, Sweden

b - Department of Biomedical and Clinical Sciences, Linköping University, Linköping, Sweden

c - CNRS, Univ Paris Est Creteil, Univ Gustave Eiffel, UMR 8208, MSME, Créteil F-94010, France

d - Paul Scherrer Institut, Villigen PSI, Switzerland

e - Division of Solid Mechanics, Lund University, Lund, Sweden

f - Department of Physics, Chalmers University, Gothenburg, Sweden

g - Center of X-ray Analytics, Empa, Swiss Federal Laboratories for Materials Science and Technology, St.Gallen, Switzerland

h - Department of Orthopaedics, Sahlgrenska University Hospital, Gothenburg, Sweden

Corresponding author. hanna.isaksson@bme.lth.se.

<https://doi.org/10.1016/j.matbio.2022.11.006>

Abstract

The specific viscoelastic mechanical properties of Achilles tendons are highly dependent on the structural characteristics of collagen at and between all hierarchical levels. Research has been conducted on the deformation mechanisms of positional tendons and single fibrils, but knowledge about the coupling between the whole tendon and nanoscale deformation mechanisms of more commonly injured energy-storing tendons, such as Achilles tendons, remains sparse. By exploiting the highly periodic arrangement of tendons at the nanoscale, *in situ* loading of rat Achilles tendons during small-angle X-ray scattering acquisition was used to investigate the collagen structural response during load to rupture, cyclic loading and stress relaxation. The fibril strain was substantially lower than the applied tissue strain. The fibrils strained linearly in the elastic region of the tissue, but also exhibited viscoelastic properties, such as an increased stretchability and recovery during cyclic loading and fibril strain relaxation during tissue stress relaxation. We demonstrate that the changes in the width of the collagen reflections could be attributed to strain heterogeneity and not changes in size of the coherently diffracting domains. Fibril strain heterogeneity increased with applied loads and after the toe region, fibrils also became increasingly disordered. Additionally, a thorough evaluation of radiation damage was performed. In conclusion, this study clearly displays the simultaneous structural response and adaption of the collagen fibrils to the applied tissue loads and provide novel information about the transition of loads between length scales in the Achilles tendon.

© 2022 The Author(s). Published by Elsevier B.V. This is an open access article under the CC BY license (<http://creativecommons.org/licenses/by/4.0/>)

Introduction

Achilles tendons transduce forces from the gastrocnemius soleus muscle complex to calcaneal bone, allowing energy efficient movement of the foot. Their viscoelastic mechanical behavior and intrinsic properties are directly connected to their complex hierarchical structure [1,2]. The main

constituents of tendons are water (55-70 % of wet weight) and collagen (60-85 % of dry weight). The collagen type I molecules (approximately 300 nm long triple helices) assemble into fibrils, organized in a quarter stagger arrangement at a periodic distance (d-spacing) of approximately 67 nm. The d-spacing includes a gap region (space in-between collagen molecules) and an overlap region (where collagen

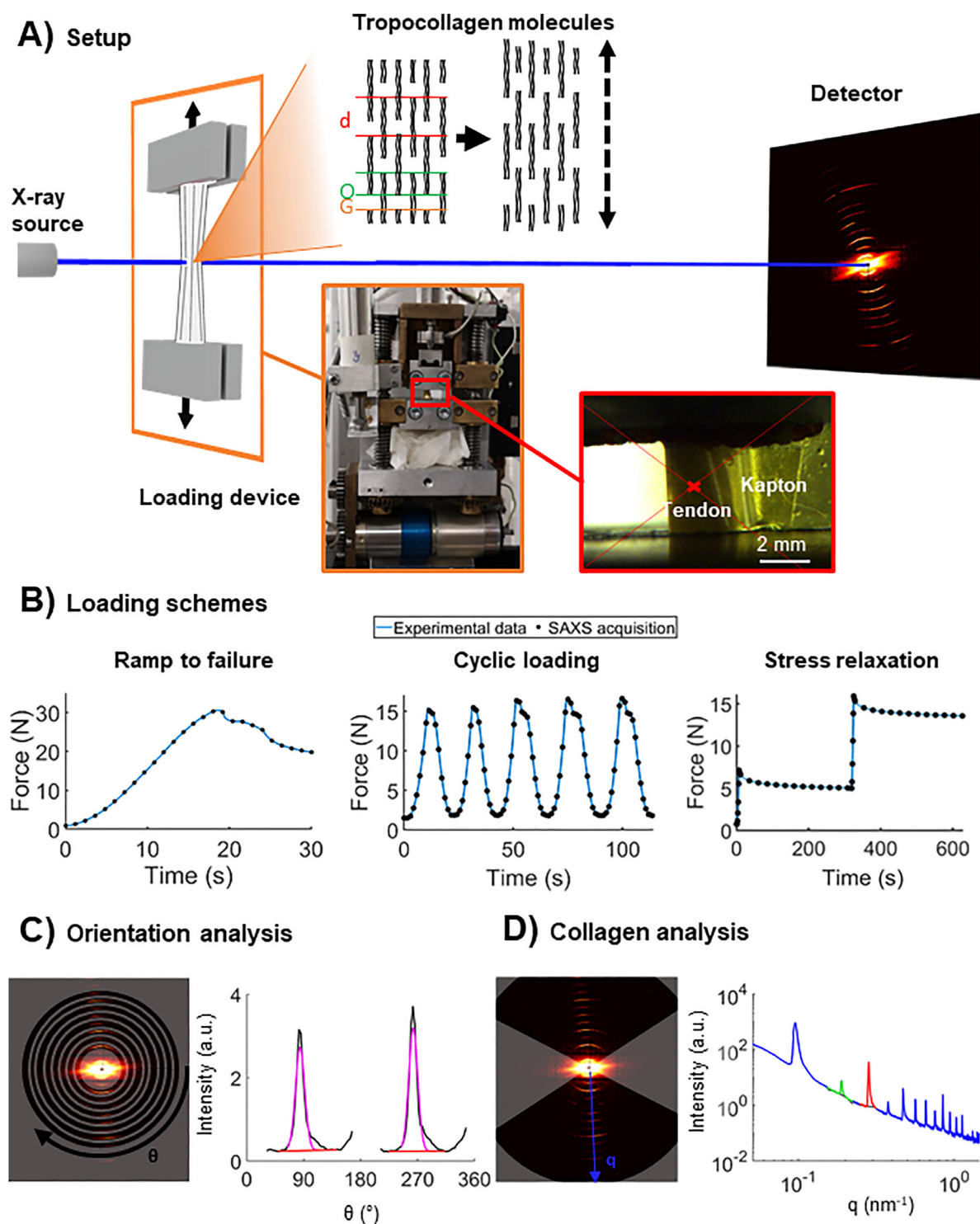


Fig. 1. Schematic of the methodology implemented in this study. A) Illustration of the combined SAXS and *in situ* loading setup, indicating the d-spacing (d), gap (G) and overlap (O) regions in the unstretched fibril state and how these change during loading. Picture showing the tendon mounted in the loading device and a representative zoom-in as visualized with the microscope, indicating the position for SAXS acquisition (red cross). B) Representative applied load curves. C) The q-regions used (not shaded) for obtaining the intensity as a function of angle $I(\theta)$ (black - smoothed data, purple - Gaussian fit, red - background). D) The q-region used (not shaded) for obtaining the intensity as a function of the q-vector $I(q)$ (blue), indicating the peaks originating from the 2nd (green) and 3rd reflection (red).

molecules overlap and are crosslinked) [3]. This quarter-staggered arrangement of molecules makes up the sub-unit of collagen [4,5]. The fibrils (~ 100 nm) assemble into fibers (~ 10 μm), that in turn assemble into fascicles and subs-tendons (~ 500 μm), and together with the interfascicular matrix, ultimately constitute the whole tendon. The mechanical properties and behavior of the whole tendon is a result of optimization at and between these hierarchical levels [1,2]. Due to the complexity of this relation, the strain transfer between different levels as well as the different deformation mechanisms behind the tissue properties and behavior, are still not completely understood.

As collagen fibrils are arranged in a highly periodic arrangement, they can be probed using X-ray diffraction techniques such as small- and wide-angle X-ray scattering (SAXS and WAXS) [5–7]. Using synchrotron radiation, these techniques have been applied during *in situ* loading, i.e. tensile loading of the full tendon while simultaneously conducting scattering measurements, to assess real-time collagen deformation mechanisms, which has led to the currently accepted concepts of fibril elongation through collagen molecule extension, elongation of

gap regions and relative sliding of adjacent molecules [7–11]. In these studies, the fibril strain has been observed to be lower than the applied tissue strain, implying that strain is being partitioned between length scales, very likely through interfibrillar sliding [12] or the interfibrillar matrix is supporting parts of the load [13]. At larger strains, there has been indications of loss of intrafibrillar order [14], and macroscopic failure has been observed to be preceded by interfibrillar sliding and damage [15]. In studies conducting mechanical testing of dissected single fibrils, however, larger fibril strains between 11–27% have been observed [16–19], with fibrils from Achilles tendons straining slightly less than e.g. tail tendons [18,19]. This indicates that the fibrils themselves can deform substantially more than they do when interconnected and assembled into larger functional units such as fascicles [8,9].

Despite the extensive research in the field of collagen mechanics, the characteristics and timing of key aspects and events during collagen nano-response to loading remain debated, and the relation to the tissue scale is not completely understood. Further, most studies have used fascicles from the rat tail tendon as a model of collagen mechanics

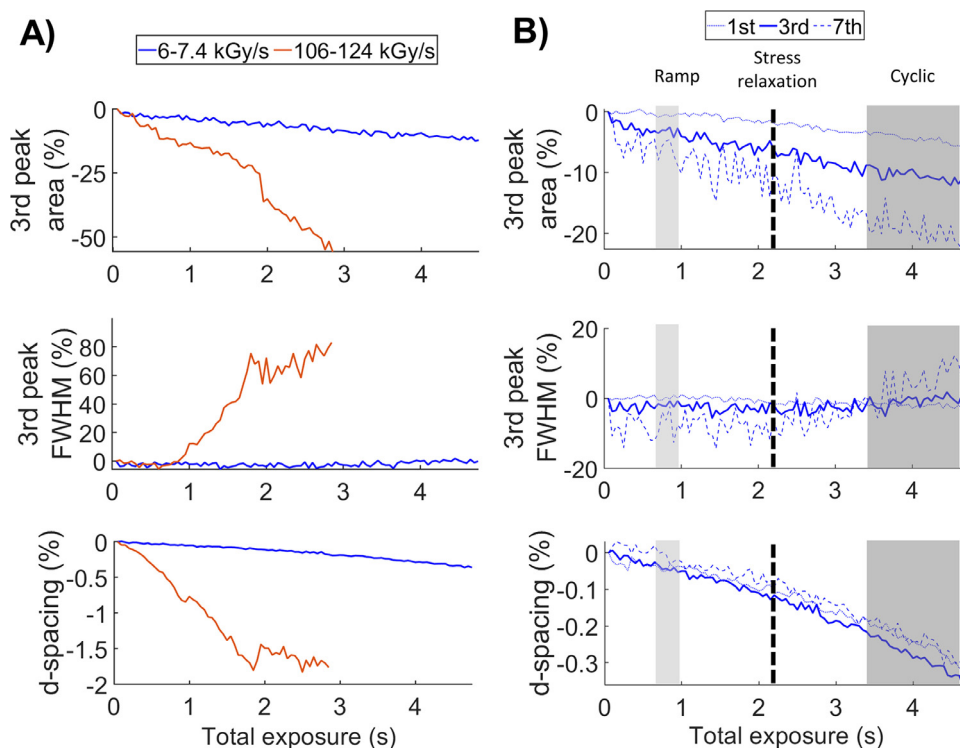


Fig. 2. Radiation damage. The effect of dose rate and total exposure time on some of the collagen structural parameters for one sample. A) Changes in collagen structural parameters for the two dose rates. A clear change in 3rd peak width (FWHM) is observed after 0.6 s. B) The effect on the 1st, 3rd and 7th meridional collagen Bragg peaks from using a dose rate of 6-7.4 kGy/s, which was selected for the remaining study. The shaded areas (vertical bars) indicate the range of maximum exposure during the mechanical tests. For instance, exposure time ranged from 0.75 to 0.95 s among specimens during the ramp to failure tests.

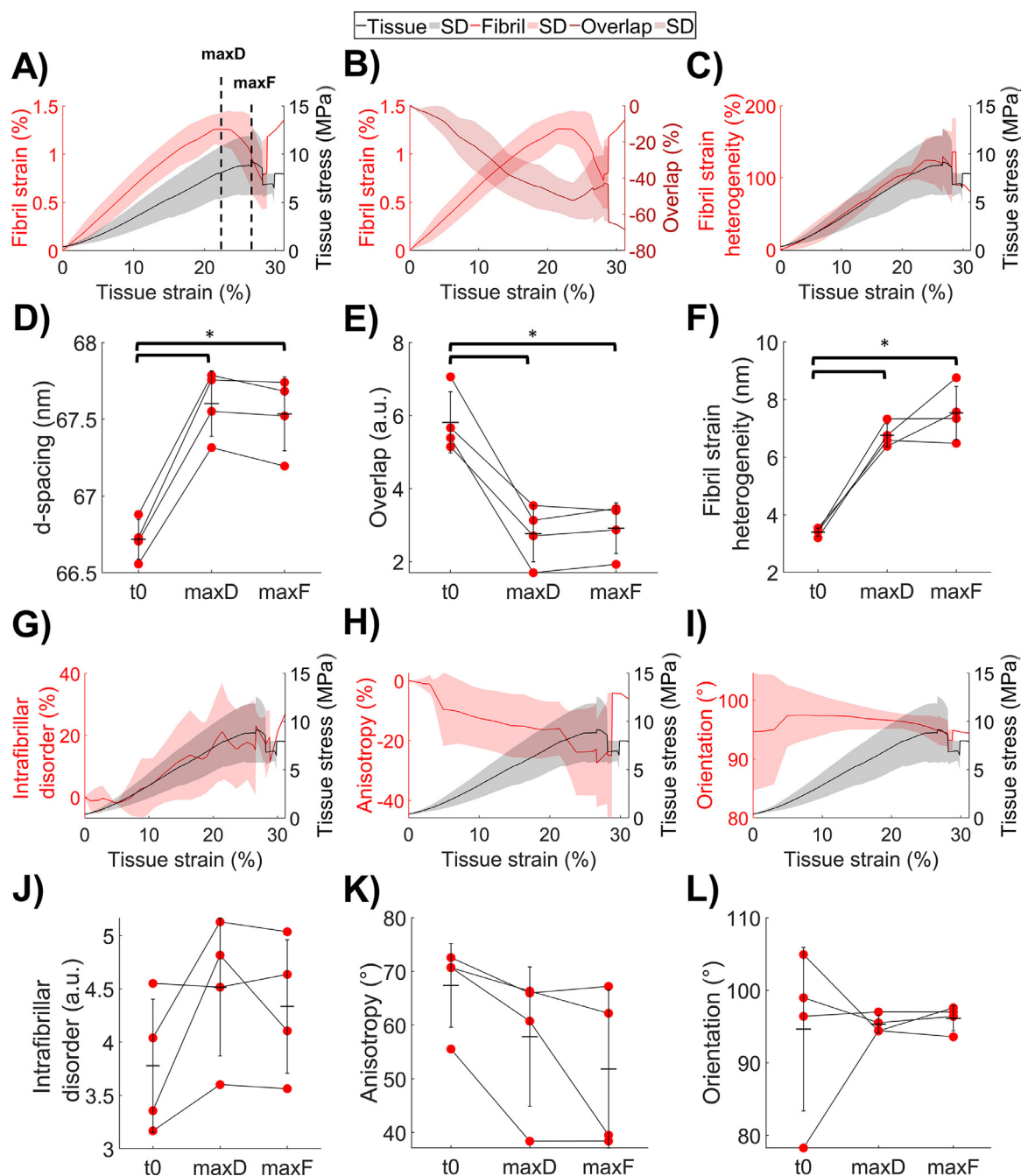


Fig. 3. Fibril response during ramp to failure. A-C and G-I) Collagen fibril structural responses during *in situ* loading. Data is shown as mean (solid line) and standard deviation (shaded area). The tissue stress is shown in black, whereas fibril parameters are shown in red. D-F and J-L) Comparison between absolute values of collagen fibril structural parameters at the start of loading (t_0), point of maximum d-spacing (maxD) and maximum tissue force (maxF). Error bars represent 95% confidence interval and statistical difference based on Kruskal Wallis test is indicated by * $p < 0.05$.

[5·7–11·13·20–22]. In addition to fascicles not being representative of the whole tendon, tail tendons are positional tendons and therefore experience the mechanical environment differently compared to energy-storing tendons [23]. In the case of energy-storing tendons, the literature is sparse. The differences in mechanical properties and response

between positional and energy-storing tendons have been highlighted in numerous studies [19·23–29]. For example, energy-storing tendons seem to rely heavily on fiber reorganization and fibril relaxation during tissue stress relaxation [23] and accumulate less fatigue induced fibril damage [28]. Contrariwise, positional tendons seemed to have

less capacity for this type of response and experience more plastic and accumulated fatigue damage. However, it remains debated if these differences extend down to the single nanoscale collagen fibril. While one study on single fibril mechanics showed similarities between collagen fibrils from positional and energy-storing tendons despite their difference in cross-linking [18], another study showed differences in both the single fibril response and in some mechanical properties [19]. Thus, there is still a lack of knowledge regarding these processes and the relation between length scales in complex energy-storing tendons such as the Achilles tendon, which is one of the most commonly injured tendons in humans [30].

The aim of this study was to characterize collagen nano-structural deformation mechanisms in rat Achilles tendons and to determine how changes in collagen fibril arrangement relate to the tissue-level mechanical behavior. Specifically, we aimed to evaluate both elastic and viscoelastic behaviors at the collagen fibril level vs the tissue scale. This was achieved through a combination of SAXS and simultaneous *in situ* tensile loading to quantify structural response at the nanoscale and to elucidate to what extent collagen fibrils align, stretch, slide, and fail in response to different tissue loading protocols (Fig. 1). Additionally, a radiation damage test was conducted prior to mechanical testing to ensure that the repeated SAXS exposure would not significantly affect the collagen structure.

Results

Radiation damage

During the radiation damage test conducted prior to the loading tests, the d-spacing and peak area displayed a gradual decrease already from the first exposure (Fig. 2.A, see Methods for details on experimental setup and analysis). With a dose rate of 106-124 kGy/s ($32 \times 20 \mu\text{m}^2$ beam size) (Fig. 1. A), a severe change in peak width (full-width-at-half-maximum, FWHM) was observed after around 0.6 s of cumulated exposure, which corresponds to a total dose of approximately 64-74 kGy. This dose level is slightly lower than previously reported values for structural damage of collagen in breast tissue (approximately 100 kGy) [44]. In relation to this, the total dose which initiated clear changes in the collagen structure in this study seemed reasonable. Thus, a beam size of $150 \times 125 \mu\text{m}^2$ was chosen, which corresponded to a dose rate of approximately 6-7.4 kGy/s. This resulted in an estimated total dose of 4.5-7 kGy during ramp to failure, 13-16 kGy during stress relaxation and 21-34 kGy during cyclic loading (Fig. 2.B). Within the total doses for the different

loading schemes, small structural changes occurred in the collagen fibrils compared to the changes induced by loading. Thus, it was assumed that the majority of the results from this study were not severely influenced by radiation damage.

Ramp to failure

During *in situ* SAXS with simultaneous tensile loading in a ramp to failure configuration, macroscopic failure occurred at tissue stresses of 9.1 ± 2.3 MPa and strains of 27 ± 1.7 %. One sample was excluded from all analysis due to visual slipping. The elastic modulus within the linear region was 45 ± 10 MPa. Within the elastic region, the fibril strain increased linearly with tissue strain (Fig. 3.A). The fibrils within the probed volume showed a decrease in slope close to global tissue yield (Supporting information, Fig. S.1) and then fibril strains rapidly decreased after reaching maximum fibril strains of 1.3 ± 0.1 %. Generally, increased loading resulted in a decrease in the length of the overlap region (Fig. 3.B,E). Further, the fibril strain heterogeneity increased with the applied load (Fig. 3.C,F). The intrafibrillar disorder showed a slight initial decrease within the toe region (-4.8 ± 2.4 %) (Fig. 3.G), which then increased as loading continued. Increased loading was also accompanied by a small increase in alignment of the collagen fibrils (i.e., a decrease in anisotropy, Fig. 3.H,K) and a slight reorientation of the fibrils towards the direction of the applied load (90°) (Fig. 3.I,L). The responses of each individual sample can be found in the Supporting information, Fig. S.2. The physiological implications of the observed fibril responses are summarized in Table 1.

Cyclic loading

During *in situ* SAXS with simultaneous tensile loading in a cyclic configuration, increasing number of load cycles resulted in an increase in tissue

Table 1. Observed fibril responses during ramp to failure and their physiological implications. Arrows indicate increase (\uparrow) or decrease (\downarrow) and (*) indicate statistical significance.

Collagen structural parameter	Physiological implication
d-spacing / fibril strain \uparrow	Collagen fibrils stretching (*)
Length of overlap region \downarrow	Collagen molecules sliding relative each other (*)
Fibril strain heterogeneity \uparrow	Wider range of fibrils carrying different loads (*)
Intrafibrillar disorder \uparrow	Loss of crystallinity / regular arrangement
Anisotropy \downarrow SD of orientation \downarrow	Collagen fibrils aligning

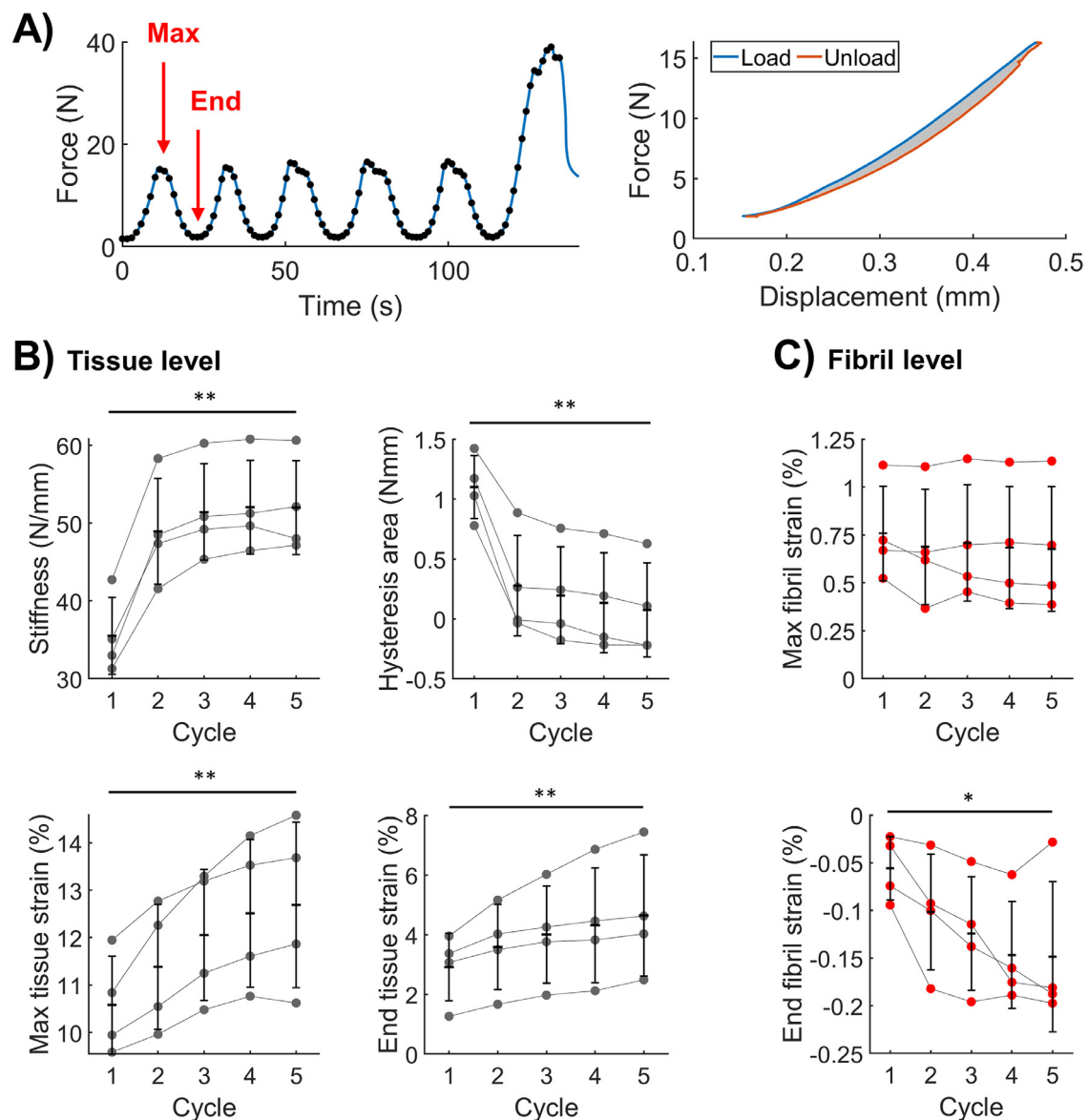


Fig. 4. Changes in tissue and fibril parameters during cyclic loading A) Representative force vs. time curve, indicating the maximum and final values of each cycle, and representative hysteresis curve, indicating the hysteresis area (grey) between the load and unload curves. B) Evolution of tissue level parameters with load cycles. C) Evolution of maximum and final fibril strain at each load cycle. The values corresponding to each individual specimen are indicated with lines. Error bars represent the 95% confidence interval and the statistical significance across all load cycles based on Friedmans test is indicated as ** $p < 0.01$ and * $p < 0.05$.

stiffness and decrease in tissue hysteresis (Fig. 4. B). Both maximum and end tissue strains also increased following number of applied load cycles. The maximum d-spacing and fibril strain measured during each load cycle remained similar (66.9 ± 0.4 nm, 0.7 ± 0.3 %). Further, the fibril strain during each load cycle was kept within the elastic region and never exceeded the failure strain observed during ramp to failure (Fig. 3.A). Contrariwise, the d-spacing and fibril strain at the end of each cycle, slightly decreased with increasing number of cycles,

with d-spacing values that were up to 0.2 % lower than the initial d-spacing at the start of loading (Fig. 4.C and Fig. 5.A). All other parameters regained their starting values following unloading at each cycle. The collagen fibril strain, length of overlap region, and heterogeneity of the fibril strain distribution adapted and responded to the applied load in a similar manner as during ramp to failure (Fig. 5.A-C). However, the response in intrafibrillar disorder and fibril alignment varied largely between specimens (Fig. 5.D-E). The physiological implications of

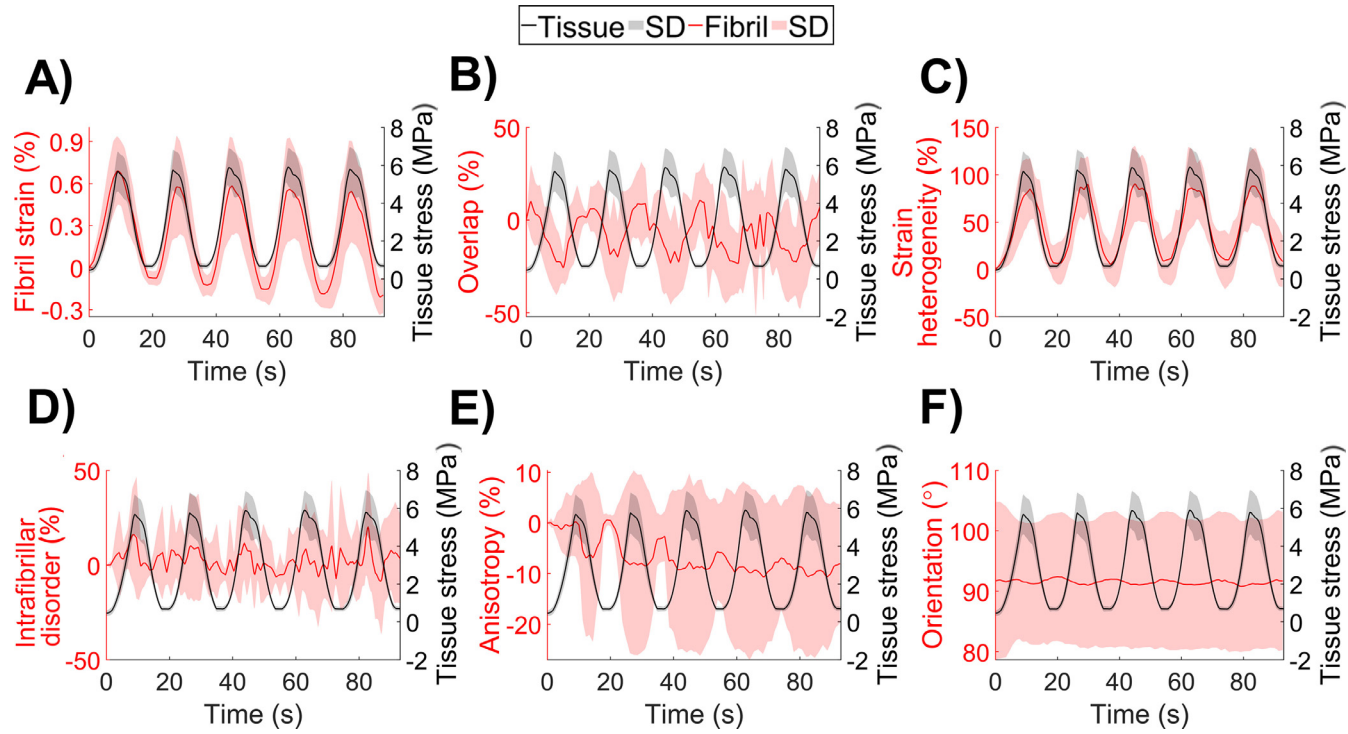


Fig. 5. Fibril behavior compared to applied force during cyclic loading. A) Fibril strain, B) length of the overlap region, C) fibril strain heterogeneity, D) intrafibrillar disorder, E) fibril anisotropy, and F) fibril main orientation. Data is shown as mean (solid line) and standard deviation (shaded area). The parameter from tissue level (force) is shown in black, whereas fibril parameters are shown in red.

Table 2. Observed fibril responses during cyclic loading and their physiological implications. Dash (-) indicates no change, arrows indicate increase (↑) or decrease (↓) and (*) indicate statistical significance.

Collagen structural parameter	Physiological implication
Max. d-spacing / fibril strain -	Collagen fibrils stretching to similar values
End d-spacing / fibril strain ↓	Collagen fibrils relaxing (*)
Length of overlap region ↓↑	Collagen molecules sliding apart and then back
Fibril strain heterogeneity ↑↓	Fibril load distribution increases and then decreases

the observed fibril responses are summarized in [Table 2](#).

Stress relaxation

During *in situ* SAXS with simultaneous tensile loading in a stress relaxation configuration, the 0.3 mm displacement steps equated to strain steps of 6.4 ± 0.4 %. Three specimens failed already during the second displacement step and are thus only included in the first step. In the remaining specimens, the stiffness and the force-relaxation ratio increased slightly between the first and the second steps ([Fig. 6.A](#)). During tissue relaxation, relaxation of the fibrils was also observed ([Fig. 6.B](#), Fibril strain). However, the other fibril parameters did not show any clear relaxation trends.

Discussion

This study combined SAXS with simultaneous *in situ* loading of whole rat Achilles tendons, to characterize the mechanical response of the collagen nanostructure in relation to the tissue scale response. The results show a clear simultaneous adaptation of the collagen structure to the applied tissue loads. Further, the combined results from the different loading scenarios indicate the extension of elastic and viscoelastic properties of the Achilles tendon down to the nanoscale.

From the radiation damage tests it was found that during the ramp to failure tests (0.75-0.95 s of beam exposure), the d-spacing reduced with approximately 0.05 %, which was only approximately 4 % of the total fibril strain due to loading. During the stress relaxation (2.2 s of beam exposure) and cyclic loading (3.5-4.6 s of beam exposure) tests, the d-spacing reduced with approximately 0.1 % and 0.2-0.3 % respectively, which both accounted to approximately 20 % of the total fibril strains due to loading. This indicates that the findings from this study were not severely influenced by radiation damage.

Loading affects intrafibrillar disorder in a bimodal manner

By measuring the area under the collagen peaks to estimate the intrafibrillar disorder, this study accounts for fibril strain heterogeneities and size of the coherently diffracting domains. The axial intrafibrillar disorder decreased within the toe region, but then increased as loading continued. This loss of intrafibrillar order could be due to the interface between the gap and overlap zones becoming less well defined [14]. Only a few studies on rat tail tendons [14,20] and cartilage [40] have previously reported the evolution of intrafibrillar order during *in situ* loading. Even though the studies on tail tendons estimated the intrafibrillar order from the peak intensity, their results are in line with this study. Misof et al. (1997) [20] observed that the lateral intrafibrillar order increased within the toe region and Fratzi et al. (1997) [14] observed a decrease of axial intrafibrillar order as the tendon is stretched into and beyond the “quasi-linear” strain range, possibly due to internal structural breakdown occurring within the fibrils. Additionally, Inamdar et al. (2017) [40] observed an increase in intrafibrillar disorder with decreasing d-spacing during compression, which is parallel to the trends seen in tendons.

Collagen peak width is related to strain heterogeneity

In the current study, the fibril strain heterogeneity started to increase at low loads and kept on increasing continuously throughout loading. This contradicts the findings in a study by Fessel et al. (2014) [9], where the fibril strain heterogeneity in rat tail tendons remained constant up until tissue yield and then suddenly increased. This discrepancy could be due to using a different displacement rate (~2.4 times faster in Fessel et al.) or the assumption that the broadening of the collagen peak is solely related to strain heterogeneity in rat tail tendons. The change in peak width could arise from two phenomena: strain and changes in the size of coherently diffracting domains [45]. To our knowledge, no study has evaluated what mechanism the broadening of the collagen peaks is attributed to. The different contributions can be obtained from a Williamson-Hall plot [46,47]. In the current study, following increased loading of the Achilles tendons, the slope of this plot increased whereas the intersect with the y-axis remained relatively constant (Supporting information, Fig. S.3). This confirms the assumption that the increase in peak width during loading in this study indeed is related to strain heterogeneity and not changes in the size of the coherently diffracting domains. Additionally, two other factors support this relation: 1) during cyclic loading, the peak width recovered during unloading and 2)

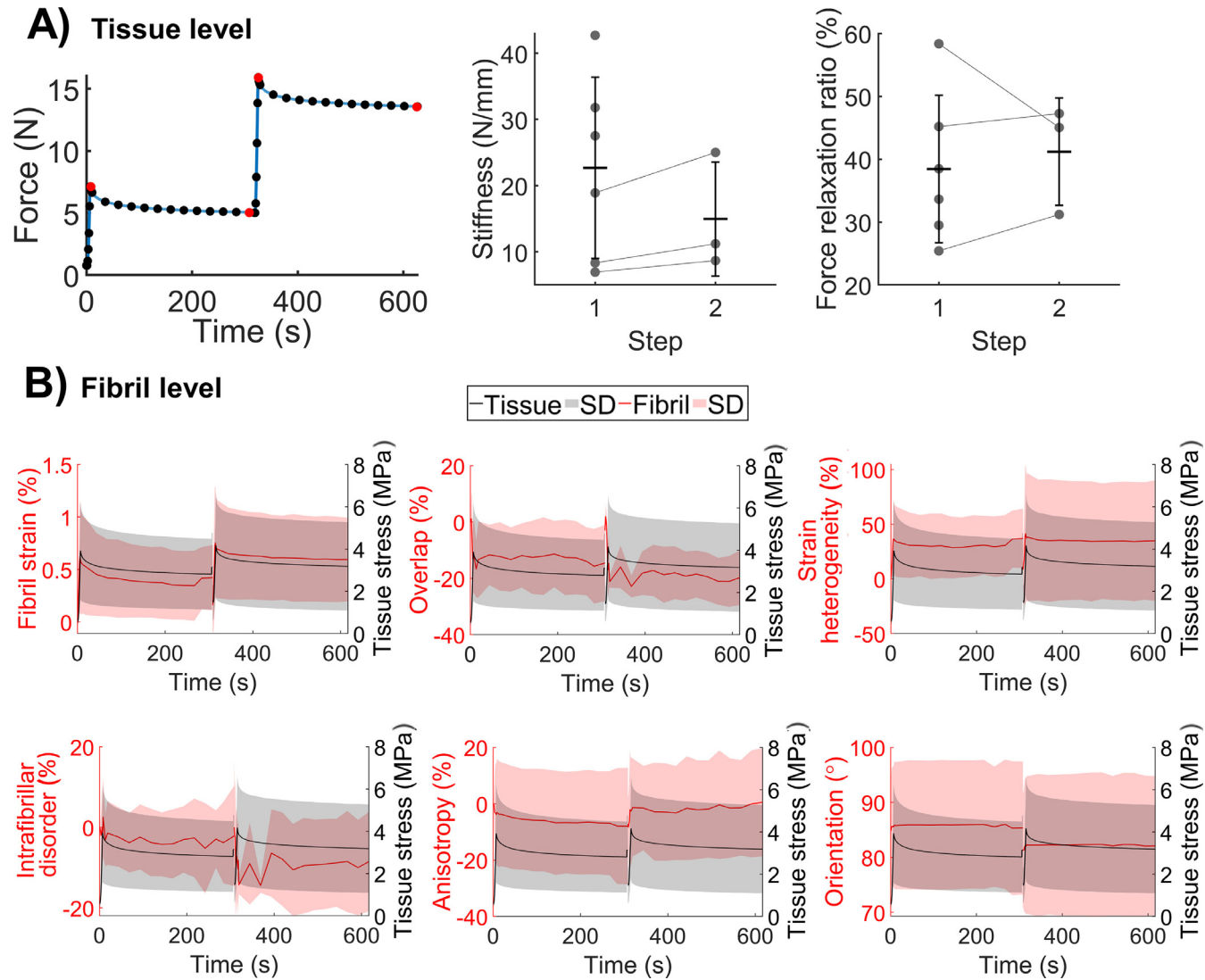


Fig. 6. Tissue and fibril behavior during stress relaxation. A) Tissue level behavior, showing a representative force time curve, indicating the maximum force and final values of each step (red dots) used for estimating stress relaxation ratios, as well as stiffness and stress relaxation ratios of each step. The values corresponding to each individual specimen are indicated with lines and error bars represent the 95% confidence interval B) Fibril level behavior during tissue relaxation. Data is shown as mean (solid line) and standard deviation (shaded area). The parameter from tissue level (force) is shown in black, whereas fibril parameters are shown in red.

during ramp to failure, the peak width recovered during unloading after tissue failure in most specimens (data not shown). Well in line with these results, Inamdar et al. (2021) [48] also observed a recovery of peak width during cyclic loading in cartilage. The sudden change in peak width reported by Fessel et al. (2014) [9], however, could instead have arisen from a sudden change in the size of the coherently diffracting domains. Additionally, non-uniform strains of the Achilles tendon have been shown, both in terms of the sub-tendons deforming differently [49,50] as well as deformation differences between the deep and superficial layers of the tendon [51,52].

Increased fibril strain recovery might not be due to damage

At lower loads within the elastic region of the tissue, the fibrils showed viscoelastic properties, such as increased fibril strain recovery and stretchability during cyclic loading. The successive decrease in d-spacing at the end of each load cycle could be attributed to one or a combination of four different factors: 1) mechanical damage to the fibrils, 2) radiation damage to the fibrils, 3) water flowing out of the structures or 4) interfibrillar matrix relaxation. As the fibril strains never exceeded the fibril yield strain, it is highly unlikely this would be due to mechanical damage. If the fibrils were damaged in any way, they would most likely also have had an increase in maximum fibril strain, since a loss in integrity of the structure would have disrupted its ability to respond to loads. Moreover, the fibril strain distribution also returned to their initial values, indicating that the size of the coherently diffracting domains was not altered. Dehydration studies of tendons have demonstrated that the d-spacing decreases with decreased humidity [39,53,54]. By evaluating the equatorial scattering peak [6,40,55] (wet state: $q \sim 1.3\text{--}1.8 \text{ nm}^{-1}$, dry state: $q \sim 1.1 \text{ nm}^{-1}$), it is possible to gain information about the intrafibrillar hydration state, but this peak could not be properly resolved with the measured q -range of this study. There are presently no studies investigating this in tendons during *in situ* loading, but Inamdar et al. (2017) [40] observed little to no change in fluid flow at the intrafibrillar level during *in situ* stress relaxation of cartilage. However, cartilage is in a state of relative dehydration compared to tendons, but the observed trend could potentially be similar. Gupta et al. (2010) [11] observed a double exponential fibril relaxation response in rat tail tendons, which they suggested was due to relaxation within the interfibrillar matrix. Hence, we hypothesize that in this study the major contributor to the observed decrease in d-spacing at the end of each load cycle was also due to interfibrillar matrix relaxation.

Tissue relaxation is accompanied by fibril relaxation

Simultaneously as the tissue underwent relaxation, fibril relaxation was observed. This is well in line with previous studies on rat tail tendons, where the fibril relaxation ratios have been shown to increase with increased strain steps [8,9]. However, no such consistent increase in relaxation ratio was found between strain steps in this study. This could be due to the limited sample numbers that were tested at step 2. Further, it could be due to the larger strain steps taken within the current study [8,9] or a too slow strain rate.

Fibril mechanical behavior within the tissue differs from single fibril mechanics

Using SAXS to evaluate fibril strains in combination with *in situ* loading of whole tendons, we and others [8–10,15,22] have observed fibril strains substantially lower than those from dissected single fibrils [16–19] (fibril failure strains $\sim 1.3\text{--}4\%$ vs $11\text{--}27\%$). However, Svensson et al. (2018) [18] observed that the fibril strain recorded at the ends ($13\text{--}14\%$ for fibrils from Achilles tendons) was increased compared to central strains as measured by optical tracking of the same fibrils ($8.5\text{--}8.9\%$), which could indicate that the strains reported in single fibril studies are slightly over-estimated. Quigley et al. (2018) [19] and Svensson et al. (2013) [16] showed that fibrils from energy storing tendons exhibit a three-phase behavior instead of the two-phased behavior observed in fibrils from positional tendons. This three-phase behavior of the collagen fibrils was not observed in this study, nor in the previous studies combining *in situ* loading with synchrotron SAXS on rat tail tendons, where the fibrils instead exhibited a linear increase in strain until they came to an abrupt decrease close to tissue yield or failure [8,9,22].

The higher fibril strains observed in single fibril studies demonstrate the capability of collagen fibrils to extend further than they do when inside the tendon. Studies based on different microscopical techniques at several parts of the tissue [56–59], indicate fibril continuity along the entire tendon. In this case, the fibril response in the full tissue should be similar to that of the single fibril. However, studies based on mechanical testing in combination with X-ray diffraction, confocal, and atomic force microscopy [11,22,60–64] strongly suggest that strain is being partitioned between the fibrils and the fibers. The strain then occurs through interfibrillar and inter-fiber shear forces, and thus suggest that the fibrils instead are functionally discontinuous. In this study, we found fibril elongation to be affected by two simultaneous mechanisms: stretching and sliding. Even though sliding was observed already at the beginning of loading, it was not as prominent during

small strains as during larger strains. This is well in line with similar studies on rat tail tendons [9,13,38] and this presence of fibril sliding further supports functional discontinuity of fibrils in the tendon. Instead, there is probably a complex coupling between different hierarchical levels, which contribute to the strain being partitioned and the single fibril thus not carrying the entire applied load. The fact that the fibrils do not reach as high strains while in this intricate arrangement could also explain why the fibrils do not reach the other phases observed in single fibrils by Quigley et al. (2018) [19] and Svensson et al. (2013) [16]. Additionally, this points towards macroscopic tissue damage and failure not being initiated within the fibrils, but rather in the structures between fibrils, fibers and sub-tendons, as implied by previous studies on fibril and fiber mechanics within full tendons or fascicles [11,22,60–62].

Comparison of energy-storing tendons and positional tendons

All of the Achilles tendons evaluated in this study had a slightly smaller d-spacing prior to loading (66.6 nm) as well as slightly lower fibril failure strains (1.3 %) compared to fascicles from rat tail tendons evaluated using the same techniques and approach (67.5–67.7 nm, 1.5–4 %) [8–10,22]. Quigley et al. (2018) [19] showed that single fibrils from positional and energy-storing tendons not only exhibited different mechanical responses, but those from energy-storing tendons were also stronger, had a higher elastic modulus and did not form kinks nor a reduction in shell delamination in response to rupture. In line with this, Svensson et al. (2018) [18] showed that fibrils from Achilles tendons strained slightly less than those from rat tail tendons. These differences could be one reason behind the d-spacing and fibril strains observed in this study being within the lower range of similar studies on rat tail tendons.

In this study, the fibrils themselves seem to exhibit plastic damage, indicated by their response shortly before failure being nonlinear (Supporting information, Fig. S.1), which in turn suggest the presence of intrafibrillar damage prior to fibril failure. The fact that the fibrils show a nonlinear response prior to fibril failure contradicts similar studies on rat tail tendons where the fibril failure was found to be abrupt and the equatorial SAXS reflections to completely disappear following tissue yield [8,9]. In this study however, whilst at a much lower intensity, the reflections remain and the d-spacing continues to change.

Neither the earlier studies on rat tail tendons [8–10,22] nor a lab-based study on explants from bovine Achilles tendons [38] related the findings to the whole tissue level, thus not considering the interplay between all hierarchical levels of the tissue. By not testing the full tissue, the strain will most likely not be partitioned as in its native state. Thus, the fibrils could

potentially experience higher loads, resulting in higher strains. Thorpe et al. (2012, 2015) [25,27] recently highlighted the major contribution of the interfascicular matrix to the overall mechanical properties. Their finding and the slight discrepancies in fibril strain levels and behavior between the current study and previous studies on rat tail tendons further emphasizes the need for studying more than one hierarchical level of the tissue at a time as well as the need for more studies on energy-storing tendons.

The discrepancies between rat tail fascicles and Achilles tendons together with the overall results of this study further highlights the heterogenous and complex response a tendon exhibit across several length scales, and this needs to be taken more often into account in mechanical studies. Future studies aimed at characterizing the mechanical response of tendons should therefore apply suitable techniques to resolve the inner mechanical heterogeneity of the tendon during loading, using e.g. SAXS or phase-contrast tomography for fibril and fiber levels respectively. Although, as this study focuses on the relation between macroscopic and nanoscale behaviors, a simplified assumption was still made for tissue scale stresses and strains.

Limitations

Compared to the physiological loading rate of tendons, the displacement rate in this study was low. Therefore, there is an uncertainty in separation between the fibril elastic response, sliding, and relaxation. Thus, more studies using a higher displacement rate need to be conducted to confirm the fibril strain values in this study. Additionally, no preconditioning was performed prior to the mechanical tests, which most likely contributes to the large inter-sample variabilities in especially the cyclic loading and stress relaxation tests. Nevertheless, all samples followed similar trends in their fibril responses. Moreover, the clamping of the tendons in this loading device could be improved as the tendons were often observed to break close to the clamps, which is most likely one reason behind the tissue failure strains and stresses of this study being relatively high and low, respectively. However, that is a common problem when performing mechanical testing of intact Achilles tendons. Additionally, the setup did not allow the tests to be conducted in a bath, but for the short measurement times in this experiment, the Kapton film was sufficient to keep the tendons hydrated throughout the tests. Lastly, the scattering data were acquired from a limited volume ($\sim 1 \times 0.15 \times 0.15 \text{ mm}^3$) in the center of the tendon and is thus averaged over many collagen fibrils in the path of the beam. Therefore, the measurements most likely do not include regional differences within the tendon, as was further confirmed with narrow, normally distributed angular intensities. In some samples however, the distribution contained a small shoulder,

indicating a slight heterogeneity within the fibril population. This could be interpreted as more than one sub-tendon being present within the beam path in these cases.

Conclusions

The powerful combination of *in situ* loading during synchrotron SAXS acquisitions enabled characterization of the relationship between the tissue and nanoscale responses in energy-storing rat Achilles tendons for both elastic and viscoelastic loading scenarios. In this study, the mechanical and functional effects of the complex hierarchical structure of the Achilles tendon were evaluated. The results show substantially lower fibril strain than the applied tissue strain and thus further support strain partitioning between hierarchical levels. Additionally, it was shown that both elastic and viscoelastic properties are transferred down to the fibril level. This study provides further insight into the non-uniform deformation mechanisms of the Achilles tendon by determining that fibril strain heterogeneity is related to changes in collagen peak width. All together, these results stress the importance and need for future studies to thoroughly consider heterogeneity when evaluating the mechanical behavior of tendons. Our approach provides the unique possibility of studying the nanostructural response of collagen fibrils within the complex arrangement of the tendon. These results could represent the basis for future studies of different pathologies or injuries affecting tendons, as well as pave the way for similar studies of other collagen-based tissues.

Methods

Samples

Female specific pathogen free (SPF) Sprague Dawley rats (N = 15), aged 10-14 weeks (weight 219 ± 21 g), were used (Janvier, Le Genest-Saint-Isle, France). The rats were kept two per cage under controlled humidity (55 %) and temperature (22° C), with a light-dark cycle of 12 hours. They were given standard food pellets and water *ad libitum*. After euthanization with carbon dioxide, the plantaris tendon was removed and the Achilles tendon was harvested together with the calcaneal bone and the gastrocnemius soleus muscle complex. The tendons were wrapped in gauze soaked in phosphate buffered saline (PBS) solution and stored frozen (-20° C) until measurements (approximately 3 months). The storage does not affect the tissue mechanics [31,32], but may cause an increased water content. The experiment adhered to the

institutional guidelines for care and treatment of laboratory animals and was approved by the Regional Ethics Committee for animal experiments in Linköping, Sweden (ID1424).

Synchrotron small-angle X-ray scattering and *in situ* loading

SAXS measurements were carried out at the coherent small-angle X-ray scattering beamline (cSAXS) at the Swiss Light Source (SLS), Paul Scherrer Institut (PSI), Switzerland. The samples were thawed, and sagittal and transverse diameters were measured with a slide caliper at the middle of the tendon. The cross-sectional area was calculated assuming an elliptical geometry. Kapton film (8 μm , 3512, SPEX Sample Prep, USA) was placed around each tendon and held together with a drop of PBS, to keep the tendon hydrated during the experiments (Fig. 1.A). The specimens were mechanically loaded at the beamline using a custom-built tensile test device designed for *in situ* measurements, similar to earlier studies [33,34]. The device was mounted on two linear stages along the two directions perpendicular to the beam path and controlled using a custom-made control software in LabVIEW (National Instruments Corp., US). During the experiment, the device was run in displacement control mode. The load was measured with a 111 N (25 lbf) load cell with an accuracy of ± 1 % (LC201 25, Omega Engineering Inc., USA). To minimize slipping, sandpaper was placed on the muscle bundle before clamping in the ribbed upper grip of the loading device, making sure that the clamps were placed below the site of visible fascicle branching. The distal end was clamped just above the calcaneal bone. Due to the design of the grips, the tendons were mounted straight, simulating extreme plantarflexion. Using a camera mounted at the beamline, a picture before and after the tests were acquired for visual evaluation of potential slippage.

The tendons were loaded in tension by equally displacing both grips simultaneously with a rate of 5 mm/min (1.8 ± 0.3 %L0/s), keeping the center of the tendon in the path of the beam and thus the measured region constant throughout the test. A force transducer measured the axial force and a linear displacement sensor recorded the displacement of the grips. All tendons were preloaded to 1 N before each loading scheme was applied. To preserve tendon hydration, no additional precondition was performed as this would have substantially prolonged the duration of the tendon being inside the experimental hutch due to limitations in the control software implementation. Three loading schemes were applied (Fig. 1.B):

- 1) ramp to failure (N = 5), where the tendons were stretched until tissue failure,

- 2) cyclic loading ($N = 4$), where 5 cycles of 2-15 N were performed,
- 3) stress relaxation ($N = 6$), where the tendons were displaced in 0.3 mm steps, followed by 300 s relaxation per step for 2 consecutive steps.

The magnitudes of cyclic force and displacement steps were chosen to be within the elastic region based on tests with the loading device prior to the experiment.

SAXS acquisitions were conducted at intervals of 1.2 s during ramp to failure and cyclic loading. During stress relaxation, 10 SAXS acquisitions were conducted at intervals of 1.2 s during the initial loading phase and early relaxation, followed by 12 SAXS acquisitions conducted at intervals of 25 s during the remaining time of the relaxation phase (Fig. 1.B).

SAXS measurements were conducted using a beam energy of 12.4 keV (wavelength of ~ 1 Å) and a sample-detector distance of 7.146 m, enabling data acquisition in the q -range of approximately 0.02 - 1.45 nm^{-1} . The sample-detector distance and beam center were determined using a silver behenate powder standard. An off-axis optical microscope calibrated with the X-ray beam position was used to find the center of the tendon, where SAXS acquisition was conducted using a beam size of 150×125 μm^2 (horizontal \times vertical) and an exposure time of 50 ms. The beam flux was measured (3.0×10^{11} photons/s) using a glassy carbon standard specimen [35]. The 2D scattering patterns were recorded with a Pilatus 2M detector (1475×1679 pixels², pixel size 172×172 μm^2). Measurements of only the Kapton film next to the samples were conducted for background correction. To investigate the effects of the dose rate on the specimens, this beam configuration was compared to a second configuration with higher number of incident X-rays onto the measured sample area, by reducing the beam size to 32×20 μm^2 and thus providing a measured flux of approximately 1.7×10^{11} photons/s.

Data analysis

Analysis of the 2D scattering patterns was performed using in-house codes in Matlab® (R2019a, MatchWorks Inc, USA) as previously described by Turunen et al. (2017) [36]. The beam stop was masked away from the scattering patterns, along with dead or over-exposed pixels and gaps between detector modules. To obtain the $I(\theta)$ curves, the scattering patterns were angularly integrated over 0 - 360° in the q -regions of the 3rd-10th meridional reflections (indicated by non-shaded areas in Fig. 1.C). The $I(\theta)$ peaks were fitted with Gaussian curves and the predominant orientation of the collagen fibrils was determined from the position of the fit (Fig. 6.C). The degree of anisotropy, i.e. the dispersion in fibril orientation, was

determined as the full-width-at-tenth of maximum (FWTM) of this fit [36,37]. The $I(q)$ scattering curves were obtained in the q -region of 0.05 - 1.45 nm^{-1} by radially integrating the scattering patterns over the retrieved main fibril orientation $\pm 60^\circ$ to cover the meridional scattering (indicated by non-shaded areas in Fig. 1.D), giving rise to peaks related to each meridional collagen reflection (blue curve in Fig. 1.D). Gaussian curves were fitted to the 1st through 10th collagen peaks of the $I(q)$ curve. The 3rd peak was used to determine the collagen periodicity (d -spacing) as the peak position and the fibril strain heterogeneity, i.e. dispersion in fibril strains, as changes in peak width (FWHM). The intensity ratio between the 3rd and 2nd peaks (I_3/I_2) was calculated from their respective peak areas and used to estimate changes in the length of the overlap region (O), which varies when adjacent collagen molecules slide relative to each other [38,39]. The relationship between relative intensity of collagen peaks of order m and n can be described by [9,10,36,38]:

$$\frac{I_m}{I_n} = \left(\frac{n}{m}\right)^2 \left[\frac{\sin(m\pi O/d)}{\sin(n\pi O/d)}\right]^2 \quad (1)$$

where I_n and I_m are the intensity of the n^{th} and m^{th} order collagen peaks respectively, O is the overlap length, and d is the d -spacing.

When a degree of disordering of the gap/overlap interface is present, the intensity of higher order peaks is reduced by a larger amount compared to lower order peaks [14,40]. This reduction can be described by applying a Debye-Waller type factor $\exp(-\kappa q^2)$, where κ is proportional to the disordering and $q_n = \frac{2\pi n}{D}$, to equation 1 [40]:

$$\frac{I_m}{I_n} = \left(\frac{n}{m}\right)^2 \left[\frac{\sin(m\pi O/d)}{\sin(n\pi O/d)}\right]^2 \exp\left(-\kappa(m^2 - n^2) \left(\frac{2\pi}{D}\right)^2\right) \quad (2)$$

The intensity ratio between the 5th and 7th order collagen peaks (I_5/I_7) was calculated from their respective peak areas and used to estimate changes in intrafibrillar disorder, which increases when the interface between gap and overlap region gets less distinct [14,40].

The force applied to the tissue was normalized to the cross-sectional area of the tendon (2.3 ± 0.7 mm^2) to obtain tissue stress (σ). Tissue strain (ε_T) and fibril strain (ε_F) were obtained by normalizing the tissue displacement and collagen d -spacing to their starting values [9]:

$$\varepsilon_T = (L - L_0)/L_0 \quad (3)$$

$$\varepsilon_F = (d - d_0)/d_0 \quad (4)$$

where L is the displaced tissue length, L_0 the initial distance between the grips at preload (4.6 ± 0.7 mm), d the d -spacing, and d_0 the initial d -spacing at

preload (66.6 ± 0.2 nm). Stiffness was determined from a fit of the linear region in the load curve and the yield point was estimated as 0.2 % strain offset from this fit (post-linear region). Hysteresis was determined per cycle as the area between the loading and unloading force-displacement curve. Stress relaxation ratio corresponded to the relative decrease in force from the start of each step until the end of the relaxation period.

Radiation damage

Radiation dose is an important and limiting factor when studying biological samples such as tendons, as too high doses can damage the tissues and especially affect their mechanical properties [41]. Thus, prior to mechanical testing, a radiation damage test was conducted on a tendon not subjected to mechanical load to ensure that the repeated SAXS exposure would not significantly affect the collagen structure. Two dose rates were compared by varying the beam size ($150 \times 125 \mu\text{m}^2$ or $32 \times 20 \mu\text{m}^2$) and repeatedly acquiring SAXS measurements at one spot. The sample transmission was estimated from the number of photons recorded at the beam stop with and without a sample in the beam path. The absorption ratio was calculated from the recorded transmission at the beam stop, as the ratio of photons not being transmitted. The tissue density was estimated to be between $1050\text{--}1120 \text{ kg/m}^3$, based on typical values reported for soft tissues such as muscle, cartilage, skin and tendons [42,43]. The total dose (D) deposited on the sample was defined as the energy absorbed by the sample divided by the sample mass, and was calculated as:

$$D = \frac{I_0 \cdot \tau \cdot A \cdot E}{\Delta_x \Delta_y \Delta_z \cdot \rho} \quad (5)$$

where I_0 is the photon flux (photons/s), τ is the exposure time, A is the absorption ratio, E the X-ray energy, $\Delta_x \Delta_y \Delta_z$ is the scattering volume (beam area \times sample thickness), and ρ the mass density of the sample.

Statistics

Mean, standard deviation (SD) and 95% confidence intervals (CI) were calculated. Non-parametric tests were selected as the number of samples was too small to ensure normally distributed data. In ramp to failure, the Kruskal-Wallis test was used to test for statistical difference between start of loading (t_0), maximum d-spacing (maxD) and maximum force (maxF) (R2019a, MathWorks Inc., USA). In cyclic loading, the Friedman's test was used to test for statistical differences across multiple load cycles.

Data Availability

The datasets generated during the current study are available in the Zenodo repository, <https://doi.org/10.5281/zenodo.7371107>.

Declarations of Competing Interest

none

Acknowledgements

This project has received funding from the Knut and Alice Wallenberg Foundation (WAF2017) and the European Research Council (ERC) under the European Union's Horizon 2020 research and innovation programme (grant agreement No 101002516). We acknowledge the European Union's Horizon 2020 research and innovation programme under grant agreement No 731019 (EUSMI), which provided beamtime at the cSAXS beamline, Paul Scherrer Institut, Switzerland, as well as the Paul Scherrer Institut and the beamline staff at cSAXS for help before, during and after the beamtime.

Supplementary materials

Supplementary material associated with this article can be found, in the online version, at [doi:10.1016/j.matbio.2022.11.006](https://doi.org/10.1016/j.matbio.2022.11.006).

Received 26 July 2022;

Received in revised form 29 September 2022;

Accepted 21 November 2022

Available online 23 November 2022

Keywords:

Achilles tendon;

Nanomechanics;

Collagen structure;

Small-angle X-ray scattering;

In situ loading

References

- [1] P. Fratzl, Cellulose and collagen: from fibres to tissues, *Current Opinion in Colloid and Interface Science*, 8, Elsevier BV, 2003, pp. 32–39.
- [2] P. Fratzl, R. Weinkamer, Nature's hierarchical materials, *Prog. Mater. Sci.* 52 (8) (2007) 1263–1334.

- [3] A. Veis, Collagen fibrillar structure in mineralized and non-mineralized tissues, *Curr. Opin. Solid State Mater. Sci.* 2 (3) (1997) 370–378.
- [4] JA Petruska, AJ. Hodge, A subunit model for the tropocollagen macromolecule, *Proc. Natl. Acad. Sci. United States* 51 (1964) 871–876.
- [5] JPRO Orgel, TC Irving, A Miller, TJ. Wess, Microfibrillar structure of type I collagen in situ, *Proc. Natl. Acad. Sci. USA* 103 (24) (2006) 9001–9005.
- [6] P Fratzl, N Fratzl-Zelman, K. Klaushofer, Collagen packing and mineralization. An x-ray scattering investigation of turkey leg tendon, *Biophys. J.* 64 (1) (1993) 260–266.
- [7] HS. Gupta, Chapter 7: nanoscale deformation mechanisms in collagen. editor. in: P Fratzl (Ed.), *Collagen: Structure and Mechanics, an introduction*, Springer US, Boston, 2008.
- [8] A Gautieri, FS Passini, U Silván, M Guizar-Sicairos, G Carimati, P Volpi, M Moretti, H Schoenhuber, A Redaelli, M Berli, et al., Advanced glycation end-products: Mechanics of aged collagen from molecule to tissue, *Matrix Biol.* 59 (2017) 95–108.
- [9] G Fessel, Y Li, V Diederich, M Guizar-Sicairos, P Schneider, DR Sell, VM Monnier, JG. Snedeker, Advanced glycation end-products reduce collagen molecular sliding to affect collagen fibril damage mechanisms but not stiffness, *PLoS One* 9 (11) (2014).
- [10] F Bianchi, F Hofmann, AJ Smith, MS. Thompson, Probing multi-scale mechanical damage in connective tissues using X-ray diffraction, *Acta Biomater.* 45 (2016 Nov 1) 321–327.
- [11] HS Gupta, J Seto, S Krauss, P Boesecke, HRC. Screen, In situ multi-level analysis of viscoelastic deformation mechanisms in tendon collagen, *J. Struct. Biol.* 169 (2) (2010) 183–191.
- [12] SE Szczesny, KL Fetchko, GR Dodge, DM. Elliott, Evidence that interfibrillar load transfer in tendon is supported by small diameter fibrils and not extrafibrillar tissue components, *J. Orthop. Res.* 35 (10) (2017) 2127–2134.
- [13] W Folkhard, E Mosler, W Geercken, E Knörzer, H Nemetschek-Gansler, T Nemetschek, MHJ. Koch, Quantitative analysis of the molecular sliding mechanisms in native tendon collagen - time-resolved dynamic studies using synchrotron radiation, *Int. J. Biol. Macromol.* 9 (3) (1987) 169–175.
- [14] P Fratzl, K Misof, I Zizak, G Rapp, H Amenitsch, S. Bernstorff, Fibrillar structure and mechanical properties of collagen, *J. Struct. Biol.* 122 (1997) 119–122.
- [15] E Knörzer, W Folkhard, W Geercken, C Boschert, MHJ Koch, B Hilbert, H Krahl, E Mosler, H Nemetschek-Gansler, T. Nemetschek, New aspects of the etiology of tendon rupture - An analysis of time-resolved dynamic-mechanical measurements using synchrotron radiation, *Arch. Orthop. Trauma Surg.* 105 (2) (1986) 113–120.
- [16] RB Svensson, H Mulder, V Kovanen, SP. Magnusson, Fracture mechanics of collagen fibrils: influence of natural cross-links, *Biophys. J.* 104 (11) (2013) 2476–2484.
- [17] RB Svensson, CS Eriksen, PHT Tran, M Kjaer, SP. Magnusson, Mechanical properties of human patellar tendon collagen fibrils. An exploratory study of aging and sex, *J. Mech. Behav. Biomed. Mater.* 124 (April) (2021) 104864.
- [18] RB Svensson, ST Smith, PJ Moyer, SP. Magnusson, Effects of maturation and advanced glycation on tensile mechanics of collagen fibrils from rat tail and Achilles tendons, *Acta Biomater.* 70 (2018) 270–280.
- [19] AS Quigley, S Bancelin, D Deska-Gauthier, F Légaré, L Kreplak, SP. Veres, In tendons, differing physiological requirements lead to functionally distinct nanostructures, *Sci. Rep.* 8 (1) (2018).
- [20] K Misof, G Rapp, P. Fratzl, A new molecular model for collagen elasticity based on synchrotron x-ray scattering evidence, *Biophys. J.* 72 (3) (1997) 1376–1381.
- [21] E Mosler, W Folkhard, E Knörzer, H Nemetschek-Gansler, T Nemetschek, MHJ. Koch, Stress-induced molecular rearrangement in tendon collagen, *J. Mol. Biol.* 182 (4) (1985 Apr 20) 589–596.
- [22] R Puxkandl, I Zizak, O Paris, J Keckes, W Tesch, S Bernstorff, P Purslow, P. Fratzl, Viscoelastic properties of collagen: Synchrotron radiation investigations and structural model, *Philos. Trans. R Soc. B Biol. Sci.* 357 (1418) (2002) 191–197.
- [23] HRC Screen, S Toorani, JC. Shelton, Microstructural stress relaxation mechanics in functionally different tendons, *Med. Eng. Phys.* 35 (1) (2013) 96–102.
- [24] CT Thorpe, C Klemt, GP Riley, HL Birch, PD Clegg, HRC. Screen, Helical sub-structures in energy-storing tendons provide a possible mechanism for efficient energy storage and return, *Acta Biomater.* 9 (8) (2013) 7948–7956.
- [25] CT Thorpe, MSC Godinho, GP Riley, HL Birch, PD Clegg, HRC. Screen, The interfascicular matrix enables fascicle sliding and recovery in tendon, and behaves more elastically in energy storing tendons, *J. Mech. Behav. Biomed. Mater.* 52 (2015) 85–94.
- [26] CT Thorpe, HL Birch, PD Clegg, HRC. Screen, Tendon physiology and mechanical behavior: structure-function relationships. Tendon regeneration: understanding tissue physiology and development to engineer functional substitutes, Elsevier Inc., 2015, pp. 3–39.
- [27] CT Thorpe, CP Udeze, HL Birch, PD Clegg, Screen HRC. Specialization of tendon mechanical properties results from interfascicular differences, *J. R. Soc. Interface* 9 (76) (2012) 3108–3117.
- [28] TW Herod, NC Chambers, SP. Veres, Collagen fibrils in functionally distinct tendons have differing structural responses to tendon rupture and fatigue loading, *Acta Biomater.* 42 (2016) 296–307.
- [29] RK Choi, MM Smith, S Smith, CB Little, EC. Clarke, Functionally distinct tendons have different biomechanical, biochemical and histological responses to in vitro unloading, *J. Biomech.* (2019) 95.
- [30] G. Hess, Achilles tendon ruptures, *Foot ankle Spec.* 3 (1) (2009) 29–32.
- [31] NP Quirk, C Lopez De Padilla, RE De La Vega, MJ Coenen, A Tovar, CH Evans, SA Müller, Effects of freeze-thaw on the biomechanical and structural properties of the rat Achilles tendon, *J. Biomech.* 81 (2018) 52–57.
- [32] F Dietrich-Zagonel, M Hammerman, M Bernhardsson, P. Eliasson, Effect of storage and preconditioning of healing rat Achilles tendon on structural and mechanical properties, *Sci. Rep.* 11 (1) (2021) 1–10.
- [33] J Engqvist, SA Hall, M Wallin, M Ristinmaa, TS. Plivelic, Multi-scale measurement of (amorphous) polymer deformation: simultaneous x-ray scattering, digital image correlation and in-situ loading, *Exp. Mech.* (2014).
- [34] A Gustafsson, N Mathavan, MJ Turunen, J Engqvist, H Khayeri, SA Hall, H. Isaksson, Linking multiscale deformation to microstructure in cortical bone using in situ loading, digital image correlation and synchrotron X-ray scattering, *Acta Biomater.* 69 (2018 Mar) 323–331.

- [35] AJ Allen, F Zhang, R Joseph Kline, WF Guthrie, J Ilavsky, NIST standard reference material 3600: absolute intensity calibration standard for small-angle x-ray scattering, *J. Appl. Crystallogr.* 50 (2017) 462–474.
- [36] MJ Turunen, H Khayyeri, M Guizar-Sicairos, H. Isaksson, Effects of tissue fixation and dehydration on tendon collagen nanostructure, *J. Struct. Biol.* 199 (3) (2017 Sep) 209–215.
- [37] H Khayyeri, P Blomgran, M Hammerman, MJ Turunen, A Löwgren, M Guizar-Sicairos, P Aspenberg, H. Isaksson, Achilles tendon compositional and structural properties are altered after unloading by botox, *Sci. Rep.* 7 (1) (2017 Dec 12) 13067.
- [38] N Sasaki, S. Odajima, Elongation mechanism of collagen fibrils and force-strain relations of tendon at each level of structural hierarchy, *J. Biomech.* 29 (9) (1996) 1131–1136.
- [39] A Bigi, AM Fichera, N Roveri, MHJ. Koch, Structural modifications of air-dried tendon collagen on heating, *Int. J. Biol. Macromol.* 9 (3) (1987) 176–180.
- [40] SR Inamdar, DP Knight, NJ Terrill, A Karunaratne, F Cacho-Nerin, MM Knight, HS. Gupta, The secret life of collagen: temporal changes in nanoscale fibrillar pre-strain and molecular organization during physiological loading of cartilage, *ACS Nano* 11 (10) (2017) 9728–9737.
- [41] HD Barth, EA Zimmermann, E Schaible, SY Tang, T Alliston, RO Ritchie, Characterization of the effects of x-ray irradiation on the hierarchical structure and mechanical properties of human cortical bone, *Biomaterials* 32 (34) (2011) 8892–8904.
- [42] FA. Duck, Mechanical properties of tissue, *Phys. Prop. Tissues* 3 (1990) 137–165.
- [43] RF. Ker, Dynamic tensile properties of the plantaris tendon of sheep (ovis aries), *Exp. Biol.* 2 (1981).
- [44] M Fernández, J Keyriläinen, R Serimaa, M Fernández, J Keyriläinen, R Serimaa, M Torkkeli, M Karjalainen-Lindsberg, M Tenhunen, et al., Related content Human breast cancer in vitro Small-angle x-ray scattering studies of human breast tissue samples. Vol. 47, *Phys. Med. Biol.* 47 (2002) 577 INSTITUTE OF PHYSICS PUBLISHING PHYSICS IN MEDICINE AND BIOLOGY *Phys. Med. Biol.*
- [45] AR Stokes, AJC. Wilson, The diffraction of x rays by distorted crystal aggregates - I, *Proc. Phys. Soc.* 56 (3) (1944) 174–181.
- [46] GK Williamson, WH. Hall, X-ray line broadening from filed aluminium and wolfram, *Acta Metall.* 1 (1) (1953) 22–31.
- [47] A Khorsand Zak, WH Abd. Majid, ME Abrishami, Yousefi R. X-ray analysis of ZnO nanoparticles by Williamson-Hall and size-strain plot methods, *Solid State Sci.* 13 (1) (2011) 251–256.
- [48] SR Inamdar, S Prévost, NJ Terrill, MM Knight, HS. Gupta, Reversible changes in the 3D collagen fibril architecture during cyclic loading of healthy and degraded cartilage, *Acta Biomater.* 136 (2021 Dec 1) 314–326.
- [49] T Finni, M Bernabei, GC Baan, W Noort, C Tijs, H. Maas, Non-uniform displacement and strain between the soleus and gastrocnemius subtendons of rat Achilles tendon, *Scand. J. Med. Sci. Sport* 28 (3) (2018) 1009–1017.
- [50] H Maas, W Noort, GC Baan, T. Finni, Non-uniformity of displacement and strain within the Achilles tendon is affected by joint angle configuration and differential muscle loading, *J. Biomech.* 101 (2020) 109634.
- [51] LC Slane, DG. Thelen, Non-uniform displacements within the Achilles tendon observed during passive and eccentric loading, *J. Biomech.* 47 (12) (2014 Sep 22) 2831–2835.
- [52] JR Franz, LC Slane, K Rasseke, DG. Thelen, Non-uniform in vivo deformations of the human Achilles tendon during walking, *Gait Posture* 41 (1) (2015) 192–197.
- [53] A Masic, L Bertinetti, R Schuetz, SW Chang, TH Metzger, MJ Buehler, P. Fratzl, Osmotic pressure induced tensile forces in tendon collagen, *Nat. Commun.* 6 (2015 Jan 22).
- [54] TJ Wess, JP. Orgel, Changes in collagen structure: Drying, dehydrothermal treatment and relation to long term deterioration, *Thermochim. Acta* 365 (1–2) (2000) 119–128.
- [55] S. Lees, Considerations regarding the structure of the mammalian mineralized osteoid from viewpoint of the generalized packing model, *Connect. Tissue Res.* 16 (4) (1987) 281–303.
- [56] PP Provenzano, R. Vanderby, Collagen fibril morphology and organization: implications for force transmission in ligament and tendon, *Matrix Biol.* 25 (2) (2006 Mar) 71–84.
- [57] RB Svensson, A Herchenhan, T Starborg, M Larsen, KE Kadler, K Qvortrup, SP. Magnusson, Evidence of structurally continuous collagen fibrils in tendons, *Acta Biomater.* 50 (2017 Mar 1) 293–301.
- [58] KM Hijazi, KL Singfield, SP. Veres, Ultrastructural response of tendon to excessive level or duration of tensile load supports that collagen fibrils are mechanically continuous, *J. Mech. Behav. Biomed. Mater.* 97 (2019) 30–40.
- [59] AS Craig, MJ Birtles, JF Conway, DAD Parry, An estimate of the mean length of collagen fibrils in rat tail-tendon as a function of age, *Connect. Tissue Res.* 19 (1) (1989) 51–62.
- [60] SE Szczesny, DM. Elliott, Interfibrillar shear stress is the loading mechanism of collagen fibrils in tendon, *Acta Biomater.* 10 (6) (2014) 2582–2590.
- [61] AH Lee, SE Szczesny, MH Santare, DM. Elliott, Investigating mechanisms of tendon damage by measuring multi-scale recovery following tensile loading, *Acta Biomater.* 57 (2017) 363–372.
- [62] F Fang, SP. Lake, Experimental evaluation of multiscale tendon mechanics, *J. Orthop. Res.* 35 (2017) 1353–1365.
- [63] BE Peterson, SE. Szczesny, Dependence of tendon multi-scale mechanics on sample gauge length is consistent with discontinuous collagen fibrils, *Acta Biomater.* 117 (2020 Nov 1) 302–309.
- [64] SE Szczesny, JL Caplan, P Pedersen, DM. Elliott, Quantification of interfibrillar shear stress in aligned soft collagenous tissues via notch tension testing, *Sci. Rep.* 5 (2015) 14649.